Antenna performance predictions of a radio telescope subject to thermal perturbations

Keith B. Doyle
MIT Lincoln Laboratory
244 Wood St., Lexington, MA 02420

ABSTRACT

Antenna performance predictions and calibration times are estimated on a 37 m diameter radio telescope subject to thermal perturbations. The telescope is designed to operate at frequencies up to 325 GHz with a one-way performance requirement of 1 dB loss in gain accounting for fabrication, alignment, gravity and thermal errors. Thermal gradients acting over the antenna structure due to diurnal air temperature variations are a significant contributor to degradations in antenna performance. Integrated thermal-structural-optical analyses were performed to predict antenna performance as a function of the diurnal variations. Based on the results, design requirements were imposed on the radome thermal control system and the rate of calibration of the hexapod mounted subreflector.

Keywords: integrated modeling, thermal-structural-optical analysis, RF error, finite element analysis, multidisciplinary modeling, optomechanical analysis

1. INTRODUCTION

The Haystack antenna, originally built over 40 years ago to operate at 8-10 GHz, is currently being upgraded to support imaging radar applications at a frequency of 96 GHz and radio astronomy at 230 GHz. The Cassegrain antenna is comprised of a 37 m parabolic primary reflector with an F/D ratio of 0.4 and a 2.84 m hyperbolic subreflector. The antenna is housed inside a 45.7 m space frame radome. The entire elevation structure including the aluminum subreflector, quadrapod, surface panels and subframes, backstructure, and the steel transition structure, is being replaced. A CAD model of the Haystack antenna is shown in Figure 1.

The primary reflector is comprised of 432 surface panels. Each fabricated panel includes a thin aluminum surface skin epoxied to longitudinal and transverse channels. A set of four or five panels are mounted to 104 individual aluminum truss structures known as subframes. The subframes are then mounted and aligned to the backstructure. The aluminum backstructure is a truss structure made from tubes and plates welded together. At the center of the backstructure is an aluminum torque ring which is attached to the steel transition structure using sixteen reflector support struts that act to minimize antenna errors due to differential thermal expansion characteristics of the aluminum and steel structures.

Critical to the performance of the antenna is maintaining the surface shape of the primary reflector subject to environmental perturbations including gravity and thermal loading. A large fraction of the gravity induced deformations in the primary reflector is compensated by repositioning the subreflector that is mounted on a six degree-of-freedom hexapod. For example, when the antenna is pointing zenith the subreflector is able to compensate for focus errors and when the antenna is pointing horizon the subreflector is able to compensate for tilt and coma surface errors.

This work is sponsored by the Department of the Air Force under Air Force contract FA8721-05-C-0002. Opinions, interpretations, conclusions, and recommendations are those of the authors and are not necessarily endorsed by the United States Government.

Operational design criteria of the antenna require a half pathlength error (HPLE) over a 10° to 40° elevation angle of 100 μm rms. The HPLE is often cast as an effective primary reflector surface error. The operational performance budget accounts for manufacturing, alignment, gravity, and thermal-induced errors of the panels, subframes, and backstructure as shown in Table 1. Additional antenna performance metrics shown in Table 1 include the antenna efficiency and the loss in gain in dB. The HPLE is commonly related to the antenna efficiency, η, using Ruze's equation:

$$\eta = e^{-(\frac{4\pi\sigma}{\lambda})^2}$$

where σ is the HPLE rms and λ the wavelength. This equation is generally valid for antenna efficiencies of 0.80 and above. The loss in gain is computed using $10\log_{10}\eta$.

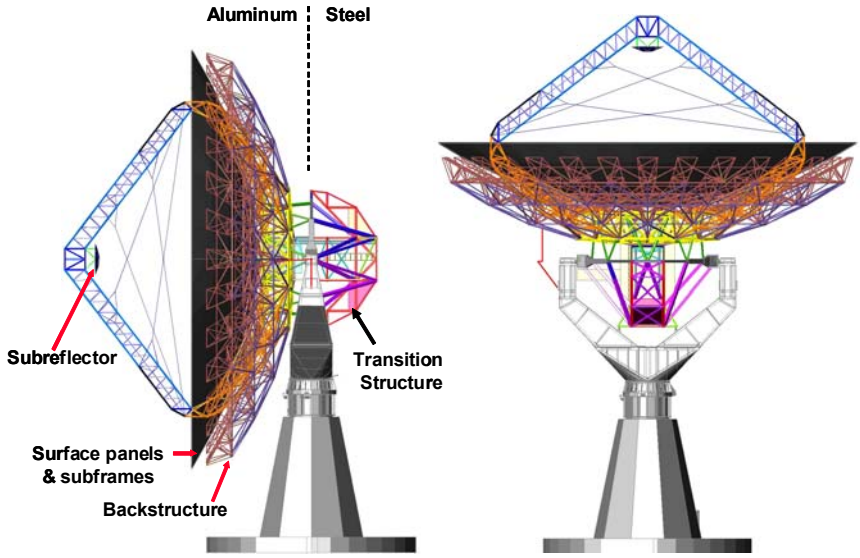

Figure 1. CAD Model of the Haystack antenna showing the major assemblies of the elevation structure.

Contributor	HPLE (um rms)	Antenna Efficiency	Gain Loss in dB
Panel Manufacturing	30	0.979	0.09
Gravity Deformation			
-Panel	12	0.997	0.015
-Subframe	5	0.999	0.0025
-Backstructure	44	0.956	0.2
Thermal			
-Panel	10	0.998	0.01
-Subframe	20	0.991	0.04
-Backstructure			
Thermal Lag (31°F)	44	0.956	0.19
Gradient (+5°F)	43	0.958	0.19
Alignment			
-Panel Setting	30	0.979	0.09
-Subframe Setting	35	0.972	0.12
Total	97.0	0.80	0.95

Table 1. Haystack antenna performance budget at an elevation angle of 10 degrees.

The two largest error budget contributors are the thermal lag and the thermal gradient errors in the backstructure. The thermal gradient allocation accounts for temperature variations across the antenna due to thermal gradients in the surrounding air within the radome. The thermal lag error is due to diurnal air temperature changes that induce gradients across the antenna structure due to the structural members' varying thermal time constants. These temperature variations across the antenna create differential expansion and contraction in the members that lead to primary reflector surface errors and errors in the position of the subreflector and the feed.

The effects of thermal lag on antenna performance were evaluated by integrating thermal, structural, and optical analyses. Temperatures for each structural member were computed as a function of time due to diurnal air temperature changes. At discrete time steps, the temperatures of the structural members were used as load cases in a thermo-elastic finite element analysis. The resulting thermo-elastic responses of the primary reflector, subreflector and feed were used to create perturbed optical models of the antenna to compute antenna performance as a function of time. Methods to decrease the thermal lag error included reducing the range of the diurnal air temperature change within the radome using a HVAC system and positioning the subreflector to optimize the gain of the antenna.

2. THERMAL ANALYSIS

Thermal gradients develop across the antenna due to variations in the thermal lag of the structural members relative to the diurnal ambient temperature changes within the radome. The quasi steady-state temperature variation, ΔT, was computed as a function of time, τ, using the following relationship based on a harmonically varying ambient temperature, T_{amb}, on the exposed surfaces of the structural member.

$$\Delta T(\tau) = T_{amb}\left[\frac{1}{\sqrt{1+(\omega/g)^2}}\cos(\omega\tau-\psi)\right] \text{ where } g=\frac{h}{\rho\cdot c_p\cdot t} \text{ and } \psi=\tan^{-1}\frac{\omega}{g}.$$

As shown, the temperature variation is dependent upon the thermal properties of the material (density and specific heat), the thermal thickness of the structural member, t, and the convection coefficient, h. The convection coefficient was assumed to be 1 Btu/(hr·ft^2·F) accounting for free convection within the radome. The thermal thickness of the structural members is computed as the ratio of the cross-sectional area over the exposed surface area with the aluminum member thermal thicknesses ranging from 0.056 to 0.57 inches and the steel members ranging from 0.17 to 1.0 inches. The above calculation assumes that the structural members are decoupled and that no heat transfer occurs across the connecting joints.

The temperatures for each of the aluminum and steel members in the elevation structure of the antenna over a 24-hour period were computed as shown in Figure 2. The member temperature variation relative to the air temperature is shown in Figure 3. At any snapshot in time, the temperature variation of the antenna members represents the thermal lag. This analysis assumed a mean temperature of 70° F with a 31° F diurnal temperature range representing the 95th percentile of air temperatures measurements recorded inside the radome over a multi-year period.

Finite element models of connection joints with varying member sizes were created to evaluate the effect of conduction through the joint on the member temperatures subject to a sinusoidal ambient air boundary condition. It was found that the majority of the length of each member responds as if the members were disconnected resulting in a slight reduction in the average temperature difference between the members. Thus excluding the heat transfer at the joint using the above analysis approach is conservative.

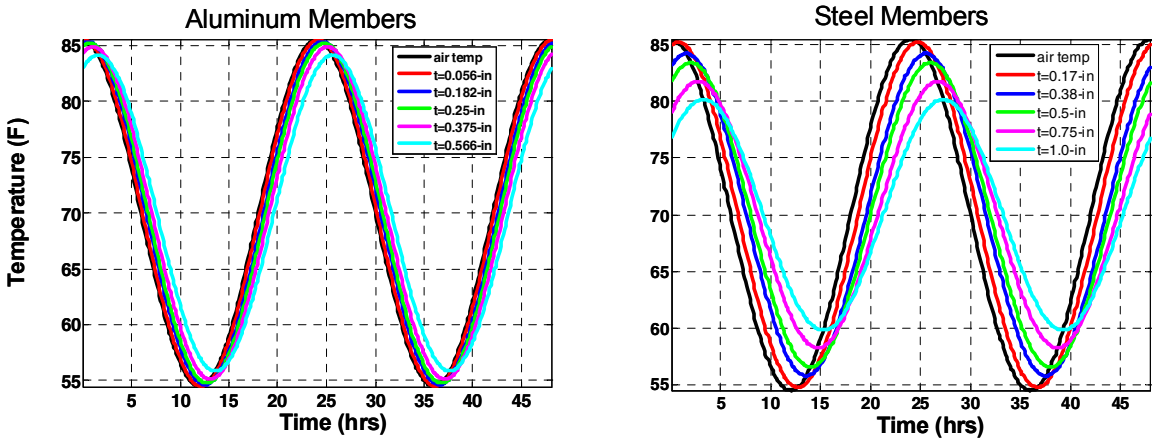

Figure 2. Thermal lag of structural members relative to daily diurnal temperature changes as a function of thickness.

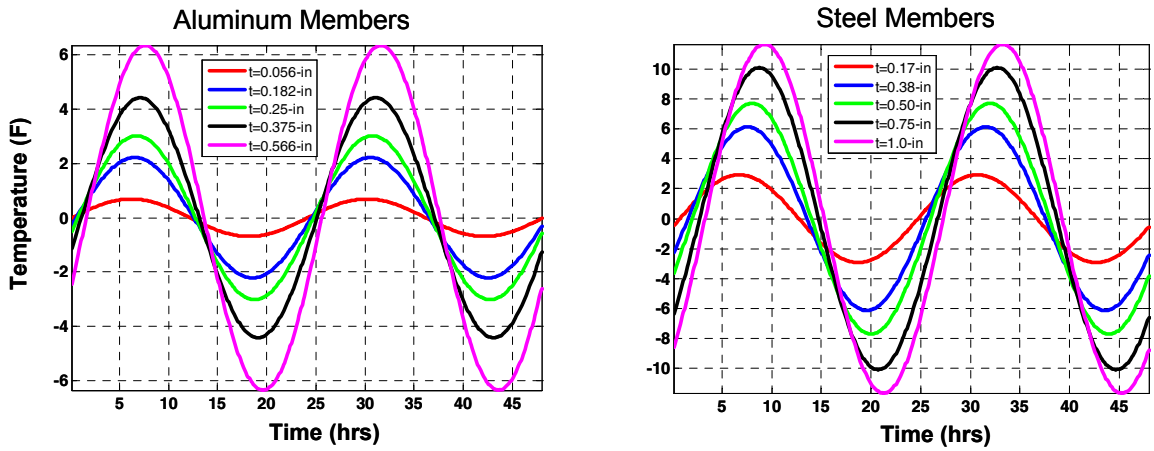

Figure 3. Thermal lag of structural members relative to the air temperature as a function of thickness.

3. THERMO-ELASTIC ANALYSIS

The thermo-elastic response of the antenna was computed using a MSC/Nastran[1] finite element model of the elevation structure which is shown in Figure 4(a). The thermal lag temperatures from the thermal analysis were imposed as load cases onto the model at one-hour increments over a 24-hour period. The surface deformations of the backstructure and the rigid-body positional errors of the subreflector and the feed were computed at each time step. A deformed shape of the finite element model is shown in Figure 4(b) with a contour plot of the deformed backstructure shown in Figure 4(c).

Because of symmetry and a homologous design, the thermal gradients induced in the structure cause predominantly changes in the radius of curvature of the primary reflector and shifts along the optical axis of both the subreflector and the feed resulting in focus changes in the antenna. Decomposing the backstructure surface deformations into Zernike polynomials using SigFit[2] reveals details of the deformed surface shape. The Zernike coefficients for the seven hour steady-state thermal lag case in units of microns is shown in Table 2. Focus is the dominant Zernike term which is consistent with the contour plot shown in Figure 4(c). This is significant since the focus error may be corrected by repositioning the subreflector. Residual surface deformations that cannot be corrected by the hexapod mounted subreflector include astigmatism, tetrafoil, and

spherical aberration. The non-axisymmetric errors are principally due to the feed box and quadrapod structure.

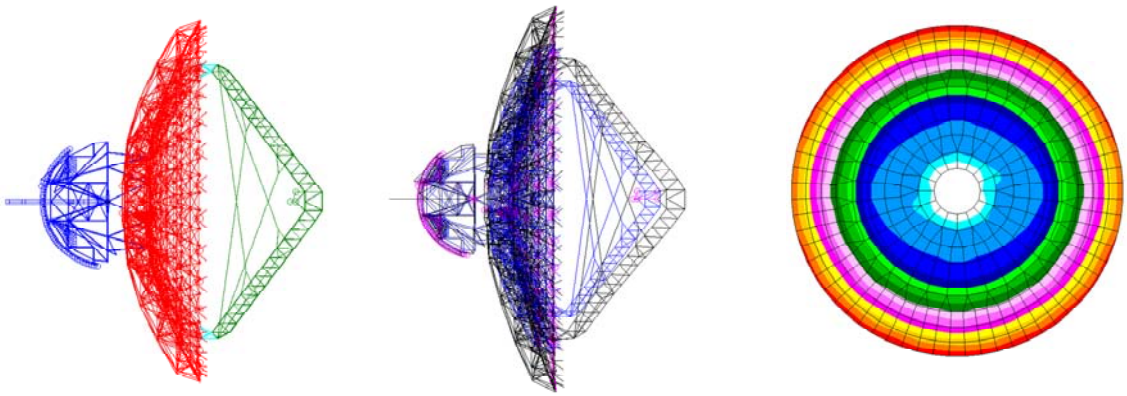

(a) (b) (c)

Figure 4. Antenna elevation structure finite element model is shown in 4(a), the deformed shape due to diurnal temperature changes in 4(b), and a contour plot of the primary reflector surface errors in 4(c).

Aberration	Magnitude (Waves)	Phi (Deg)	Residual RMS	Residual P-V
Input			398.6	1461.6
Bias	-12.0	0	398.8	1461.6
Tilt	0.0	-49.8	398.8	1461.6
Power (Defocus)	702.3	0	46.6	245.7
Pri Astigmatism	55.1	90	40.6	227.7
Pri Coma	1.5	87.2	40.6	227.1
Pri Trefoil	2.1	29.6	40.6	227.2
Pri Spherical	48.1	0	39.5	183.0
Sec Astigmatism	20.9	0.1	38.9	176.2
Pri Tetrafoil	20.4	-44.9	38.3	175.1
Sec Coma	1.5	-92.4	38.3	173.9
Sec Trefoil	0.6	29.3	38.3	173.9
Pri Pentafoil	0.1	16.3	38.3	173.9
Sec Spherical	-21.4	0	34.0	181.7
Ter Astigmatism	12.3	88.7	33.8	181.6
Sec Tetrafoil	14.6	-0.2	33.6	181.9
Pri Hexafoil	0.6	29.9	33.6	181.9
Ter Coma	1.2	85.8	33.6	181.5
Ter Trefoil	0.8	-30.4	33.6	181.4
Sec Pentafoil	0.2	-19.3	33.6	181.4
Pri Septefoil	0.0	-13.3	33.6	181.4
Ter Spherical	8.6	0	34.1	185.8

Table 2. Zernike polynomials representing primary reflector surface deformations at a steady-state time of 7 hours in units of microns.

4. ANTENNA PERFORMANCE PREDICTIONS

Antenna performance predictions due to the effects of thermal lag were computed using CODEV[3] optical design software. Thermo-elastic response quantities from the finite element model including the backstructure deformations and the rigid-body positional errors of the subreflector and feed were used to develop perturbed optical models at one hour intervals over a 24 hour period using SigFit. The primary reflector finite element surface deformations were represented in the optical model using a Standard Zernike polynomial surface. The rigid-body errors of the subreflector and feed were added as tilts and decenters. The loss in antenna efficiency was then computed for each perturbed case and the data interpolated and best fit.

The optical model and a plot of antenna performance versus time in shown in Figure 5. The maximum loss in gain is 10.6 dB occurring twice daily. This loss in gain corresponds to a half pathlength error of 309 μm rms. Both these values significantly exceed the performance budget tolerances of 0.19 dB and 44 μm rms, respectively.

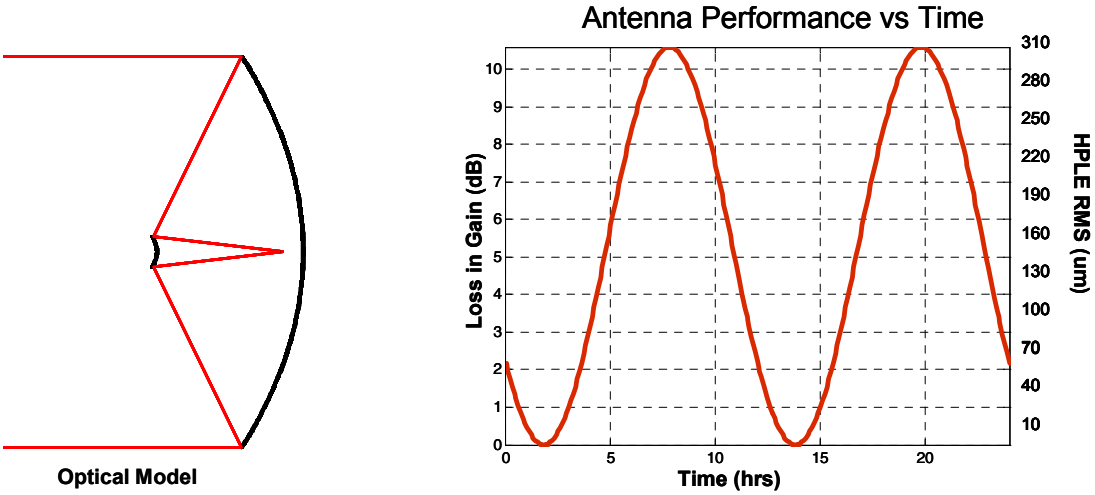

Figure 5. View of the optical model and antenna performance predictions as a function of time.

Potential solutions to reduce antenna performance loss due to thermal lag effects include axially moving the subreflector to compensate for the focus errors, controlling the thermal environments to decrease the diurnal variation inside the radome, and minimizing the difference in thermal lag between the structural members using passive or active means. This latter option includes the use of insulation to increase the thermal time constant or adding fins or blowing air across select members to decrease the thermal time constant. This latter option was ultimately discarded in favor of a combination of temperature control within the radome using a HVAC system coupled with periodic recalibrations of the subreflector position.

4. HVAC CONTROL AND ANTENNA CALIBRATION

An initial analysis was performed to determine what level of radome thermal control was required to meet the thermal lag error budget allocation assuming no repositioning of the subreflector. This analysis was performed by predicting the antenna performance for various harmonically varying air temperature ranges. The relationship between the range in diurnal air temperature and the loss in gain of the antenna is shown in Figure 6. The air temperature would need to be controlled to ± 2.5° F such that the effects of thermal lag stays within the error budget allocation.

The next analysis performed was to determine how often the subreflector needs to be recalibrated as a function of the radome diurnal variation. This relationship can then be used to establish design requirements on the HVAC system to optimize performance and cost relative to the number of subreflector calibrations. Determining how often the subreflector needs to be repositioned depends on the time of day and the residual error of the antenna. The residual error refers to the uncorrected antenna error after calibration. The antenna residual error and the shift in the axial position of the subreflector were determined by using the perturbed optical model. For each time step, the position of the subreflector was determined that minimized the HPLE of the antenna using the CODEV optimization routine.

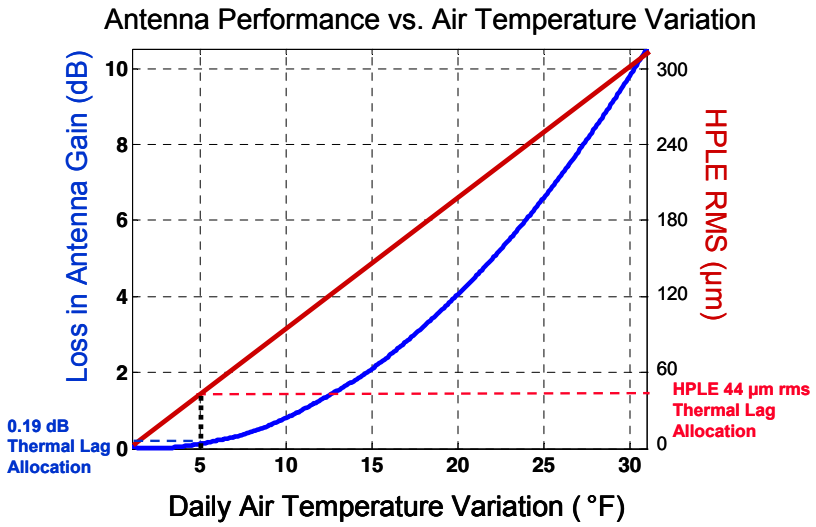

Figure 6. Loss in antenna gain versus diurnal temperature range.

Assuming continuous correction by the subreflector, the residual error of the antenna along with the axial position of the subreflector for the diurnal temperature range of 31° F is shown in Figure 7. The total range that the subreflector travels is 0.25-inches that reduces the 10.6 dB uncorrected thermal lag error to 0.18 dB - within the error budget allocation of 0.19 dB. For the diurnal change of 31° F, recalibration of the antenna must occur almost immediately at the time of maximum residual error otherwise the performance error would exceed the error budget allowable. However, at other times of the day such at the point of the minimum residual error, calibration times are increased.

Calibration times as a function of the diurnal temperature range were based upon using the rate of change in the position of the subreflector as a measure of the rate of change in the thermal lag focus error and were computed using two methods. The first method is where the antenna has no residual error but has the fastest rate of change. The second method is where the antenna has the maximum residual error and the rate of change is conservatively assumed to the fastest rate of change (see subreflector motion versus time in Figure 7).

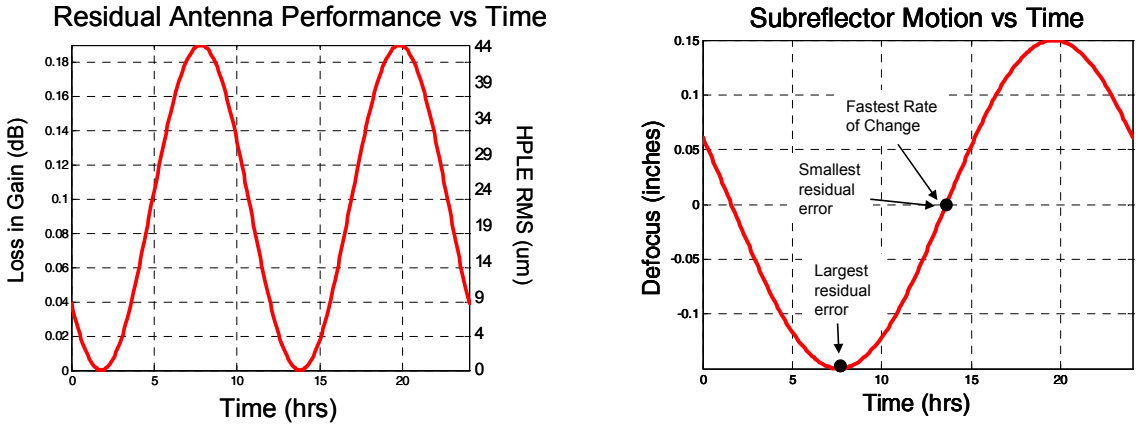

Figure 7. Antenna residual error and subreflector motion using a diurnal temperature range of 31° F.

Calibration times were computed for five diurnal temperature ranges including 31° F, 27° F, 20.25° F, 13.5° F, and 6.75° F. Note that both the residual error and the rate of change is a function of the diurnal

temperature change. The results of the analysis and the calibration times are shown in Figure 8. For a diurnal range of 31° F, the calibration time at the peak residual error is zero since any departure from this performance exceeds the error budget allocation. Conversely, starting at the point of zero residual error, the calibration time is 38.4 minutes. An initial baseline thermal control of the radome was selected to be ±10° F (total range of 20.25° F) which resulted in calibration times ranging from 44 to 61 minutes, respectively. These calibration times were well within those deemed operationally acceptable with minimal impact on the overall objectives of the antenna. As the HVAC design evolves along with cost estimates, thermal control and calibration times may be revisited.

The calibration technique axially displaces the position of the subreflector while viewing a GEO satellite or the sun to determine the optimum position to maximize the gain of the antenna. GEO satellite targets of 35 dBsm or larger are required of which several dozen currently exist in orbit. The subreflector needs to be displaced ± 0.2 inches while the antenna gain is recorded at several points. A parabolic fit would be performed on the data and the subreflector set to the peak of the fit. Calibration times are expected to be completed in less than one minute (not counting slew to/from calibration source).

Residual Error Included

Air ΔT (F)	Time(hrs)	Time(min)
31 (+/- 15.5)	0	0
27 (+/- 13.5)	0.33	19.8
20.25 (+/- 10.125)	0.74	44.4
13.5 (+/- 6.75)	1.26	75.6
6.75 (+/- 3.875)	2.5+	150+

Residual Error Excluded

Air □T (F)	Time(hrs)	Time(min)
31 (+/- 15.5)	0.64	38.4
27 (+/- 13.5)	0.77	46.2
20.25 (+/- 10.125)	1.02	61.2
13.5 (+/- 6.75)	1.45	87
6.75 (+/- 3.875)	2.5+	150+

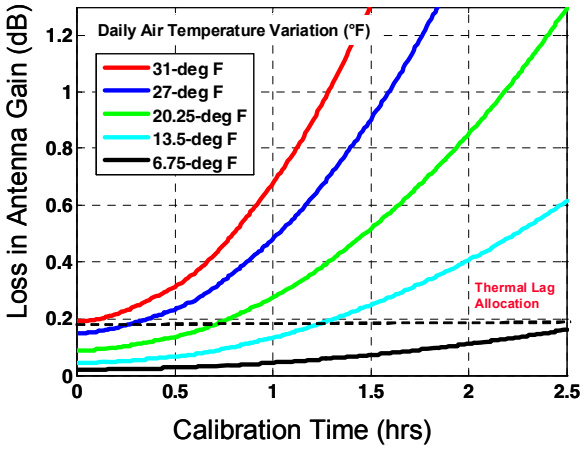

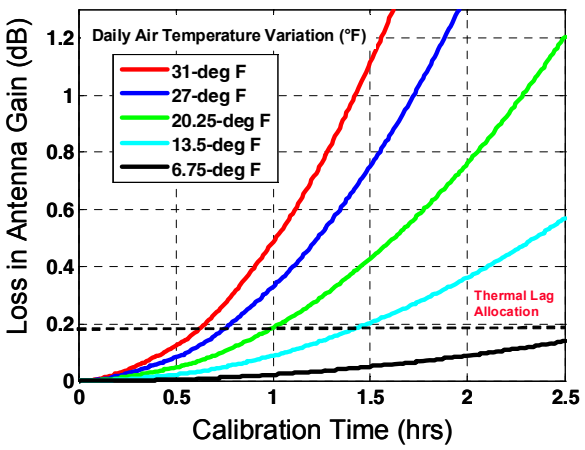

Figure 8. Calibration times are shown for both where the residual error is included and excluded.

SUMMARY

Antenna performance degradations due to thermal lag effects were predicted using integrated thermal-structural-optical analyses. Initial analyses showed that uncompensated, the effects of thermal lag significantly exceeded antenna error budget allocations and compromised performance. Solutions to minimize the effects of thermal lag included controlling the range of the radome diurnal temperature using a HVAC system and repositioning the subreflector. Recalibrating the subreflector required the antenna to use an appropriate target from which the optimum position could be inferred from a relationship of gain versus position. Subreflector calibration times versus radome diurnal temperature range were created to help determine the requirements on the HVAC system and trade performance versus operating costs. Initial baseline thermal control of the radome was selected to be ±10° F that resulted in operationally allowable

calibration times of 44 to 61 minutes. As the HVAC design evolves along with cost estimates, thermal control and calibration times may be revisited.

ACKNOWLEDGEMENTS

The author would like to acknowledge the contributions from Mike Languirand, Mark Czerwinski, Joe Usoff, Jay Eshbaugh, Phil Chapnik and Ron Efromson from MIT Lincoln Laboratory along with Joe Antebi and Frank Kann of Simpson, Gumpertz, & Heger, Inc.

REFERENCES

[1]MSC/Nastran is a registered trademark of MSC Software Corporation, Santa Ana, CA.

[2]SigFit is a product of Sigmadyne, Inc., Rochester, New York.

[3]CODEV is a registered trademark of Optical Research Associates, Pasadena, CA.